Cell Research (2017) 27:1392-1396.

www.nature.com/cr

LETTER TO THE EDITOR

An essential role for PNLDC1 in piRNA 3′ end trimming and male fertility in mice

Cell Research (2017) **27**:1392-1396. doi:10.1038/cr.2017.125; published online 10 October 2017

Dear Editor,

PIWI-interacting RNAs (piRNAs) are germ cell-specific small non-coding RNAs that are essential for silencing transposable elements. Substantial efforts in the past decade have led to an understanding of how piRNAs are made. Primary piRNA biogenesis is initiated with transcription of piRNA precursors, followed by cleavage into piRNA intermediates, and finally, maturation by 3′ end trimming and 2′-O-methylation. Secondary piRNA biogenesis occurs through an amplification loop (ping pong pathway); the piRNA pools generated through primary processing guide MILI protein to cleave the target RNA for piRNA generation in a feed-forward loop that accelerates production of the piRNAs. Papi/Tdrkh has been implicated in processing the 3′ ends of piRNAs [1, 2], however, Papi/Tdrkh lacks a recognized domain for nuclease activity. Recently, two independent studies identified the proteins that function as piRNA 3′ end trimmers in silkworms-the poly(A) specific ribonuclease PARN-1 and the PARN-like ortholog PNLDC1 [3, 4]. In *Drosophila*, instead of a PARN-like trimmer [5], a nuclease known as Nibbler that also shortens the length of piRNAs from their 3′ ends is utilized [6, 7]. The mammalian homolog of PARN is known as PNLDC1, which is a poly(A)-specific deadenylase. Here we report that deletion of *Pnldc1* results in an accumulation of 3′ untrimmed piRNA intermediates of 30~40 nt and robust expression of LINE1, which is the non-long terminal repeat (LTR) type of retrotransposons in the mouse genome. These 3′ extended pre-piRNAs still associate with PIWI proteins, but are impaired for their function. We thus demonstrate that PNLDC1 is the mouse trimmer for 3′ end maturation in piRNA biogenesis.

To investigate the function of PNLDC1 during spermatogenesis, we first detected *Pnldc1* mRNA transcripts in major organ tissues and in various stages of spermatogenesis. Quantitative RT-PCR showed that *Pnldc1* was specifically expressed in testis tissue (Supplementary information, Figure S1A). The *Pnldc1* mRNA was present in postnatal mice from 1 week to 8 weeks old (Supplementary information, Figure S1B). Moreover, the expression of *Pnldc1* in spermatogonial stem cells (SSCs) is much higher than that in pachytene spermatocytes and round spermatids (Supplementary information, Figure S1C). To investigate the *in vivo* function of *Pnldc1*, we generated *Pnldc1* mutant mice using the CRISPR/Cas9 system. Two *Pnldc1* knockout mouse lines that displayed the same phenotypes were acquired and a line containing 7 bp mutation was selected for this study (Figure 1A and Supplementary information, Figure S2A-S2F). *Pnldc1* mutant females displayed normal fertility (Supplementary information, Table S1). However, *Pnldc1* mutant males were sterile and had smaller testes with significant reduction in testis weight at 2 months of age (Figure 1B and 1C). Histological analysis revealed that adult *Pnldc1* mutants exhibited meiotic arrest (22% ± 3%) and spermiogenic defects (78% ± 3%) in round and elongating spermatids, and eventually leads to azoospermia (Figure 1D and Supplementary information, Figure S3A-S3G). No spermatozoa were observed in the lumen of the cauda epididymis of *Pnldc1* mutants (Supplementary information, Figure S3E-S3F). TUNEL assay revealed dramatically increased apoptosis (Supplementary information, Figure S3H-S3I). In order to define meiotic defects, we analyzed the assembly of synaptonemal complexes (SC) by immunolabeling the spermatocytes with antibodies against SYCP3 and SYCP1, two elements for lateral and central axis of the SC. The proportions of spermatocytes at the leptotene and zygotenestages were increased in *Pnldc1* mutant testes (Supplementary information, Figure S4A-S4B). Meiotic recombination is initiated with the formation of DNA double-strand breaks (DSBs) at the leptotene stage, which can be visualized by a DSBs marker γH2AX. In *Pnldc1*-deficient pachytene spermatocytes, although γH2AX decorated the sex chromatin, the immunolabeling of γH2AX extended onto autosomes (Figure 1E). Furthermore, electron microscopic studies showed uncondensed chromatin or abnormal retention of residual cytoplasm around the nucleus of late-stage spermatids in *Pnldc1* mutants (Figure 1F). These results suggest that *Pnldc1* mutant mice exhibited defects in

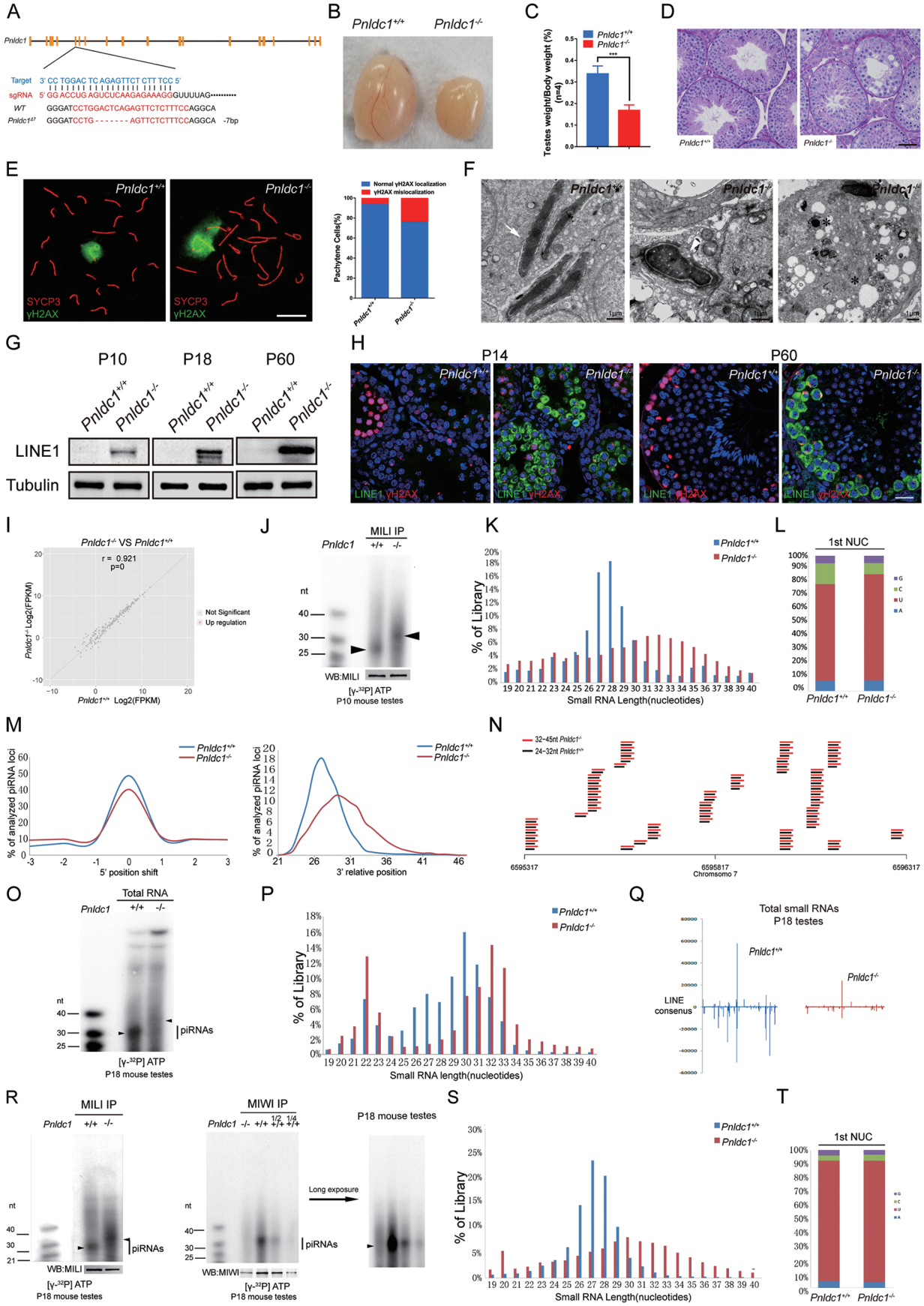
A
Pnldc1
Target 3' CC TGGAC TC AGAGTTCT CTT TCC 5'
sgRNA 5' GG ACCUG AGUCUCAAGAGAAAGGGUUUUAG
WT GGGATCCTGGACTCAGAGTTCTCTTTCCAGGCA
Pnldc1^47 GGGATCCTG - - - - - - - AGTTCTCTTTCCAGGCA -7bp
B
Pnldc1+/+ Pnldc1-/-
C
Pnldc1+/+
Pnldc1-/-
***
Testes weight/Body weight (%) (n=4)
D
Pnldc1+/+
Pnldc1-/-
E
Pnldc1+/+
Pnldc1-/-
SYCP3
γH2AX
Normal γH2AX localization
γH2AX mislocalization
Pachytene Cells(%)
F
Pnldc1+/+
Pnldc1-/-
1μm
G
P10 P18 P60
Pnldc1+/+ Pnldc1-/- Pnldc1+/+ Pnldc1-/- Pnldc1+/+ Pnldc1-/-
LINE1
Tubulin
H
P14 P60
Pnldc1+/+
Pnldc1-/-
LINE1 γH2AX
I
Pnldc1-/- VS Pnldc1+/+
r = 0.921
p=0
Not Significant
Up regulation
Pnldc1-/- Log2(FPKM)
Pnldc1+/+ Log2(FPKM)
J
MILI IP
Pnldc1 +/+ -/-
nt
40
30
25
WB:MILI
[γ-32P] ATP
P10 mouse testes
K
Pnldc1+/+
Pnldc1-/-
% of Library
Small RNA Length(nucleotides)
L
1st NUC
G
C
U
A
Pnldc1+/+ Pnldc1-/-
M
Pnldc1+/+
Pnldc1-/-
% of analyzed piRNA loci
5' position shift
3' relative position
N
32~45nt Pnldc1-/-
24~32nt Pnldc1+/+
6595317
6595817
6596317
Chromosome 7
O
Total RNA
Pnldc1 +/+ -/-
nt
40
30
25
piRNAs
[γ-32P] ATP
P18 mouse testes
P
Pnldc1+/+
Pnldc1-/-
% of Library
Small RNA length(nucleotides)
Q
Total small RNAs
P18 testes
Pnldc1+/+
Pnldc1-/-
LINE consensus
R
MILI IP
Pnldc1 +/+ -/-
nt
40
30
21
piRNAs
WB:MILI
[γ-32P] ATP
P18 mouse testes
MIWI IP
Pnldc1 -/- +/+ 1/2 +/+ 1/4 +/+
nt
40
30
25
piRNAs
WB:MIWI
[γ-32P] ATP
P18 mouse testes
Long exposure
P18 mouse testes
S
Pnldc1+/+
Pnldc1-/-
% of Library
Small RNA Length(nucleotides)
T
1st NUC
G
C
U
A
Pnldc1+/+ Pnldc1-/-

meiosis and spermiogenesis.

The piRNA pathway is essential for silencing retrotransposon activity in mouse testes. In *Pnldc1* mutant testes, an increase in LINE1(L1) transcripts was observed at postnatal day 18 (P18) (Supplementary information, Figure S5A).Western blot analysis showed that the abundance of L1 ORF1p, a protein product of active L1 elements, was already elevated in P10 *Pnldc1*$^{-/-}$ testes and increased to a much higher level at P60 (Figure 1G). L1 derepression was also confirmed by immunofluorescence detection of L1 ORF1p (Figure 1H). However, the expression level of IAP, the LTR type of retrotransposons, was similar in wild type and *Pnldc1*$^{-/-}$ testes (Supplementary information, Figure S5A). Thus, deletion of *Pnldc1* resulted in derepression of LINE1 retrotransposons. Secondary biogenesis pathway is most active in the embryonic/perinatal male germline, and the nuclear localization of MIWI2 is dependent on piRNA loading. However, L1 was not activated in *Pnldc1* mutant from P0 testes (Supplementary information, Figure S5B), and the nuclear localization of MIWI2 was observed in *Pnldc1* mutant testes at P0 (Supplementary information, Figure S5C), indicating MIWI2 was normally loaded.

To address the role of PNLDC1 in piRNA biogenesis, we first deep sequenced total small RNA populations (15~45 nt) from wild-type and *Pnldc1* mutant testes at P10, an early time point when L1 transposons were increased. Small RNAs with the size of 24-30 nt from 19 top pre-pachytene piRNA clusters were substantially decreased by 72.51% in *Pnldc1* mutant testes compared to those in wild-type testes, whereas the abundance of 31~36 nt small RNAs derived from those clusters showed three-fold increase on average (Supplementary information, Figure S6A), indicating severe defects in piRNA biogenesis. Pre-pachytene piRNA biogenesis starts with transcription of primary piRNA precursors, and the reduced mature piRNAs in *Pnldc1* mutant testes could be a result of the defect in precursor processing. Therefore, we carried out deep sequencing of the transcriptome to determine the expression level of piRNA precursors. No significant changes in the expression levels of precursors were observed (Figure 1I), indicating that the transcription and stability of piRNA precursors was not affected by *Pnldc1* depletion. Consistent with this, RT-PCR analysis revealed a similar abundance of pre-pachytene piRNA precursor (pre-cluster 10) in wild-type and *Pnldc1* mutants (Supplementary information, Figure S6B). P10 testes only express MILI protein and pre-pachytene piRNAs. We next recovered MILI RNPs from P10 wild type and *Pnldc1* mutant testes and examined their associated piRNAs by 5′ end labeling. Strikingly, MILI-bound piRNAs were dramatically reduced in the *Pnldc1* mutant (Figure 1J). Instead, the sizes of MILI-associated small RNAs were shifted to 30-40 nt (Figure 1J). Reduction of piRNAs (~28 nt reads) and a shift to longer lengths were also confirmed by deep sequencing of 15-45 nt MILI-associated RNAs from P10 testes (Figure 1K). Mapping of MILI-associated piRNA species to transposon consensus revealed a slight reduction in piRNA reads that mapped to sense Line1 sequences in the mutant (Supplementary information, Figure S6C). These longer RNA species (31-40 nt) in *Pnldc1* mutant were strongly biased for uridine at the first position (Figure 1L), suggesting that they were processed at 5′ ends in the same way as mature piRNAs, but their 3′ ends were untrimmed. To test this hypothesis, we analyzed the perfect matches for the clus-

Figure 1 PNLDC1 is required for piRNA 3′ end trimming and male fertility. **(A)** Schematic diagram of targeting strategy by CRISPR/Cas9. **(B-C)** Testis size and testis weight of wild-type and *Pnldc1*$^{-/-}$ mice at 8-week-old. n = 3-4, ***P < 0.001. **(D)** Periodic acid-Schiff (PAS) staining of testis sections from *Pnldc1*$^{+/+}$ and *Pnldc1*$^{-/-}$ mice at 8 weeks of old. **(E)** Immunolabeling of SYCP3 (red) and γH2AX (green) was performed on spread nuclei of pachytene spermatocytes from wild-type and *Pnldc1*$^{-/-}$ testes, and the quantification of γH2AX mislocalization (*Pnldc1*$^{+/+}$, n = 105; *Pnldc1*$^{-/-}$, n = 90). Scale bar, 10 μm. **(F)** Electron micrograph analysis of wild-type and *Pnldc1*-deficient elongated spermatids. Highly condensed chromatin of elongated spermatids in wild-type (white arrows), uncondensed chromatin (white arrowheads) and residual cytoplasm (asterisks) in elongated spermatids from *Pnldc1* mutants. Scale bar, 1 μm. **(G)** Western blot analysis for LINE1 (L1ORF1p) protein levels in P10, P18 and P60 testes. n = 3-4. **(H)** Immunofluorescence detection of L1ORF1p from P14 and P60 testes. **(I)** Relative abundance of 233 piRNA generating long single-strand transcripts in P10 *Pnldc1*$^{-/-}$ testes compared with *Pnldc1*$^{+/+}$ testes by transcriptome deep-sequencing (n = 3). **(J)** Testis lysates from P10 *Pnldc1*$^{+/+}$ and *Pnldc1*$^{-/-}$ mice were subjected to immunoprecipitation with anti-MILI antibody, followed by detection of MILI-associated RNAs through 5′ labeling. n = 10-11. **(K-L)** Length distribution **(K)** and the nucleotide preference at the first position **(L)** of MILI-associated RNAs from P10 mice. **(M)** The 5′ and 3′ variation analysis of piRNAs derived from the top 19 pre-pachytene piRNA clusters in P10 *Pnldc1*$^{+/+}$and *Pnldc1*$^{-/-}$ testes. **(N)** Alignments between mature piRNAs in P10 *Pnldc1*$^{+/+}$ testes and longer piRNA species in P10 *Pnldc1*$^{-/-}$ testes within a 1-kb window of piRNA cluster on chromosome 7. Mature piRNAs showed in black, longer piRNA species showed in red. **(O)** 5′ labeling of total small RNAs in P18 *Pnldc1*$^{+/+}$ and *Pnldc1*$^{-/-}$ testes. **(P-Q)** Length distribution **(P)** and reads mapped to transposon consensus **(Q)** of total small RNAs reads in P18 *Pnldc1*$^{+/+}$ and *Pnldc1*$^{-/-}$ testes. **(R)** MILI- or MIWI-associated RNAs were examined by immunoprecipitation and 5′ labeling. n = 3-4. **(S-T)** Length distribution **(S)**, and the nucleotide composition at the first position **(T)** of MILI-associated RNAs from P18 mice.

ter-derived MILI-associated piRNAs of 24-32 nt from wild-type testes in the cluster-derived 32-45 nt small RNA library of *Pnldc1* mutant. Those perfect matches were determined under the rules that they share precisely aligned 5′ ends with MILI-bound piRNAs from *Pnldc1* mutant. Our search revealed perfect matches for 39% of MILI-bound piRNAs of 24-45 nt reads that derived from the top 19 postnatal pre-pachytene piRNA clusters in *Pnldc1* mutant (statistically analyzed in Figure 1M, exemplified in Figure 1N). These results strongly suggest that the longer RNA species in *Pnldc1* mutants correspond to piRNA intermediates before 3′ end trimming.

Pachytene piRNAs are a distinct class of piRNAs that emerge in mouse testes at P14, and their biogenesis is mainly dependent on primary pathway [8, 9]. Similar to our findings with pre-pachytene piRNAs, the mature pachytene piRNAs were drastically reduced in *Pnldc1* mutant testes at P18 (Figure 1O), and this was also confirmed by deep sequencing of total small RNA populations (15-45 nt) from P18 testes (Figure 1P). Small RNAs of 24-32 nt that belong to the top 19 pachytene piRNA clusters were reduced, on average, by 88.41% (Supplementary information, Figure S7A). Mapping of total small RNAs to transposon consensus revealed a robust reduction in small RNA reads that mapped to LINE1 sequences in the mutant (Figure 1Q). Sequence annotation revealed that total small RNA reads mapped to sense-strand exonic reads in the *Pnldc1* mutant increased at the expense of reads mapped to the intergenic regions (Supplementary information, Figure S7B). We also examined the expression levels of piRNA precursors in P18 *Pnldc1* mutant testes through deep sequencing of the transcriptome, and found no apparent changes (Supplementary information, Figure S7C). RT-PCR confirmed that the precursors of three pachytene piRNAs (piR1, piR2, piR3) were expressed at similar levels in P18 wild type and *Pnldc1* mutant testes (Supplementary information, Figure S6B), while the same transcripts accumulated substantially in the testes of mice with conditional ablation of *Mov10l1,* a gene that was previously implicated in the primary processing of pachytene piRNAs (Supplementary information, Figure S6B) [10]. P18 testes express both MILI and MIWI proteins. We immunoprecipitated MILI and MIWI from P18 wild type and *Pnldc1* mutant testes, and analyzed their associated RNAs by 5′ end labeling. The near absence of MILI piRNAs and a shift to longer lengths were also observed in *Pnldc1* mutant from P18 testes (Figure 1R). Surprisingly, MIWI-bound RNAs were almost absent in *Pnldc1* mutant testes (Figure 1R). Western blot and immunofluorescence analysis revealed a dramatic reduction in MIWI protein abundance (Supplementary information, Figure S8B-S8C), suggesting that the diminished MIWI piRNAs could be a direct consequence of limited MIWI protein available to bind piRNAs in *Pnldc1* mutants. However, unlike *Miwi* knockouts that uniformly arrested at the round spermatid stage, *Pnldc1* mutant mice contained elongating spermatids in seminiferous tubules, showing a milder phenotype. Although MIWI protein was dramatically reduced, there was still a small amount of MIWI protein present in chromatoid body (Supplementary information, Figure S8C). After longer exposure of MIWI piRNAs from P18 mutant testes, residual untrimmed piRNAs could be detected. This suggests that residual MIWI proteins associate with untrimmed piRNAs to partially function in spermiogenesis. Reduction of MILI piRNAs (~28 nt reads) and a shift to longer lengths were also confirmed by deep sequencing of MILI-associated RNAs from P18 testes (Figure 1S). Moreover, RNA species bound by MILI in *Pnldc1* mutant testes were also strongly biased for uridine at the first position (Figure 1T). We next examined the consequences of longer pre-piRNAs/loss of mature piRNAs on the localization of piRNA pathway components including MILI, MIWI, TDRD1, TDRD6 and TDRKH. Strikingly, these proteins predominantly accumulated on one edge of the nucleus in *Pnldc1*-deficient pachytene spermatocytes (Supplementary information, Figure S8A). Concomitantly, mitochondria were mislocalized based on immunostaining for MT-CO1 and electron microscopy analysis (Supplementary information, Figure S8A and S8D).

In summary, here we show that *Pnldc1*-deficient mice exhibit spermatogenic defects in meiosis and spermiogenesis, which are accompanied by LINE1 activation. We demonstrated that PNLDC1 is required for the 3′ end maturation of piRNAs by processing 30-40 nt pre-piRNAs into mature piRNAs. The 5′ end of untrimmed pre-piRNAs in the *Pnldc1* mutant perfectly match the mature piRNAs and possess the strong bias for uridine at the first position. Although these longer piRNAs can still be loaded onto MILI protein, their function is impaired. piRNAs guide PIWI protein to selectively scan the germline transcripts through sequence complementarity. The extended base-pairing posed by the longer piRNAs in the *Pnldc1* mutant might decrease the efficiency of target engagement, resulting in failure to silence the L1 transposon and male sterility. However, female *Pnldc1* mutants display normal fertility, which is also observed in several piRNA pathway mouse mutants with Line1 upregulation. These results indicate that female fertility is independent of piRNA-guided Line1 repression. PNLDC1 belongs to the CAF1 family, and it is the mouse homolog of *C. elegans* PARN. Therefore, PNLDC1/PARN-1 has a conserved role in 3′ trimming during piRNA maturation.

Acknowledgments

This work was supported by the National Key R&D Program of China (2016YFA0500902 and 2017YFA0103803), the National Basic Research Program of China (2015CB943003), National Natural Science Foundation of China Grant (81471502, 31771651, 31471228), Excellent Youth Foundation of Jiangsu Scientific Committee(grant BK20150047), and Innovative and Entrepreneurial Program of Jiangsu Province. We thank Jingdi Hu (Shanghai Biotechnology Corporation, Shanghai, China) for small RNA analysis.

Yue Zhang[1, *], Rui Guo[1, *], Yiqiang Cui[1, *], Zhiping Zhu[1, 2 *], Yingwen Zhang[1], Hao Wu[1], Bo Zheng[1], Qiuling Yue[1], Shun Bai[1], Wentao Zeng[1], Xuejiang Guo[1], Zuomin Zhou[1], Bin Shen[1], Ke Zheng[1], Mingxi Liu[1], Lan Ye[1], Jiahao Sha[1]

[1]State Key Laboratory of Reproductive Medicine, Nanjing Medical University, Nanjing, Jiangsu, 210029, China; [2]The People's Hospital of Gaochun, Nanjing, Jiangsu 210029, China

*These four authors contributed equally to this work.
Correspondence: Jiahao Sha[a], Lan Ye[b], Mingxi Liu[c]
[a] E-mail: shajh@njmu.edu.cn
[b] E-mail: lanye@njmu.edu.cn
[c] E-mail: mingxi.liu@njmu.edu.cn

References

1 Saxe JP, Chen M, Zhao H, *et al*. *EMBO J* 2013; **32**:1869-1885.
2 Honda S, Kirino Y, Maragkakis M, *et al. RNA* 2013; **19**:1405-1418.
3 Tang W, Tu S, Lee HC, *et al. Cell* 2016; **164**:974-984.
4 Izumi N, Shoji K, Sakaguchi Y, *et al. Cell* 2016; **164**:962-973.
5 Czech B, Hannon GJ. *Cell* 2016; **164**:838-840.
6 Feltzin VL, Khaladkar M, Abe M, *et al. Aging Cell* 2015; **14**:443-452.
7 Wang H, Ma Z, Niu K, *et al. Development* 2016; **143**:530-539.
8 Girard A, Sachidanandam R, Hannon GJ, *et al*. *Nature* 2006; **442**:199-202.
9 Aravin A, Gaidatzis D, Pfeffer S, *et al. Nature* 2006; **442**:203-207.
10 Zheng K, Wang PJ. *PLoS Genet* 2012; **8**:e1003038.

(**Supplementary information** is linked to the online version of the paper on the *Cell Research* website.)